Earth, Planets and Space
a SpringerOpen Journal

LETTER Open Access

A transmission electron microscope study of Itokawa regolith grains

Lindsay P Keller[1*] and Eve L Berger[2]

Abstract

Analyses of two olivine-rich particles from asteroid 25143 Itokawa returned by the Hayabusa mission (RA-QD02-0125 and RA-QD02-0211) show evidence for space weathering processes that occurred in the Itokawa regolith. Submicrometer impact-derived crystalline and glassy grains are observed adhering to the surfaces of the particles, including albite, orthopyroxene, olivine, augite, pyrrhotite, troilite, melt splashes, and melt spherules. Both particles are surrounded by 50- to 100-nm-thick disordered rims that are nanocrystalline, not amorphous, and compositionally similar to the grain cores. A pyrrhotite grain attached to RA-QD02-0125 also shows a disordered rim that is sulfur-depleted with nanophase Fe metal grains decorating the outermost surface. The structurally disordered rims on the Hayabusa particles likely result from atomic displacement damage from solar wind ions given the similarity of the rim thickness compared to the implantation depth of solar wind ions. The outermost few nanometers of the disordered rims are more Si-rich and Mg- and Fe-depleted relative to the cores of the grains and likely represent a minor accumulation of impact-generated vapors or sputter deposits. Nanophase Fe metal particles are present in the rim on RA-QD02-0211 but were not detected in the rim on RA-QD02-0125. Solar flare particle tracks are observed in RA-QD02-0211 but were not observed in RA-QD02-0125, suggesting short surface exposure times for the particles, on the order of approximately 10^3 to 10^4 years. This result implies that the optical effects of space weathering develop far more rapidly than was previously recognized.

Keywords: Hayabusa; Itokawa; Space weathering; Irradiation; Micrometeorite impact; Solar flare tracks; Transmission electron microscopy

Findings

Background

In a remarkable engineering achievement, the JAXA space agency successfully recovered the Hayabusa spacecraft in June 2010, following a non-optimal encounter and surface sampling mission to asteroid 25143 Itokawa. So far, several thousand regolith grains have been recovered from the collection canister (e.g., Tsuchiyama et al. 2011). These are the first direct samples ever obtained and returned from the surface of an asteroid, and the Hayabusa samples thus present a special opportunity to directly investigate the evolution of asteroidal surfaces, from the development of the regolith to the study of space weathering effects.

Preliminary analyses of the Hayabusa samples show that their mineralogy and composition are consistent with an LL5-LL6 ordinary chondrite parent body with some less equilibrated LL4 petrographic-type material (Nakamura et al. 2011). Because they directly sample the optical surface of Itokawa, the Hayabusa samples hold the key to resolving one of the most vexing problems in cosmochemistry: identifying the asteroidal sources of ordinary chondrites, the most abundant type of meteorites (Chapman 2004). The mineralogy of asteroids is largely inferred by matching their visible near-IR reflectance spectra with those obtained from meteorites. However, the optical properties of airless bodies in the Solar System are modified over time through exposure to the space environment by a group of processes known as space weathering. Space weathering modifies the reflectance spectra of materials by attenuating absorption features, changing the spectral slope (reddening), and lowering albedos.

* Correspondence: Lindsay.P.Keller@nasa.gov
[1]Robert M Walker Laboratory for Space Science, Code KR, Astromaterials Research and Exploration Science, NASA Johnson Space Center, Houston, TX 77058, USA
Full list of author information is available at the end of the article

These spectral changes obscure the underlying mineralogy of the bodies to such an extent that direct spectral matches between asteroids and meteorites are generally difficult to impossible. Spacecraft encounters, laboratory modeling, and analyses of gas-rich meteorites and lunar samples have yielded insights into asteroidal space weathering processes, but the detailed chemical and mineralogical alteration of asteroidal surfaces is still uncertain (Gaffey 2010).

The surface of Itokawa has regions of both coarse and finer-grained material. The locations of the finer-grained material correspond to areas with gravitational potential lows; this material may have concentrated by seismic shaking (Miyamoto et al. 2007). The coarser regions that include large boulders with distinct morphologies, many of which appear to be breccias, suggest a complex collisional history (Noguchi et al. 2010). No well-defined large craters are present, but numerous micrometeroid impact pits (centimeter-sized and smaller) are observed on boulder surfaces in the highest-resolution images (Abe et al. 2006; Miyamoto et al. 2007; Takeuchi et al. 2009).

Abe et al. (2006) presented near-infrared spectral data for Itokawa showing surface variations of up to 10% in absorption band depths and albedo that result from differences in space weathering effects and physical properties (e.g., grain size). Hiroi et al. (2006) explored these variations through modeling and showed that different amounts of nanophase Fe metal ($npFe^0$) produced via space weathering could account for the albedo and absorption depth variations. Noguchi et al. (2011) showed transmission electron microscope (TEM) data from several Hayabusa grains (olivine and pyroxene) with surfaces decorated with $npFe^0$ as well as nanophase FeS grains (presumably troilite). These nanophase inclusions were all <5 nm in diameter, similar to the size distribution observed in vapor-deposited rims on lunar soil grains and much smaller than those in agglutinitic melt glass (Keller and Clemett 2001). Major questions remain regarding the origin of these space-weathered components - are they deposits of material sputtered from neighboring grains or vapors condensing from nearby micrometeorite impacts? Noguchi et al. (2011) described space-weathered surface layers up to 60-nm thick, similar to those on lunar soil grains that accumulate in 10^4 to 10^6 years. If the rims on the Hayabusa grains are formed through radiation processes, then one would also expect solar flare track densities to be similar to those in lunar grains with analogous rims (e.g., Zhang and Keller 2011).

While several Hayabusa grains have evidence of space weathering effects on their surfaces, they also have some unexpected properties (Noguchi et al. 2011, 2013). Here we report on our preliminary TEM measurements on two Itokawa samples.

Methods

We were allocated particles RA-QD02-0125 and RA-QD02-0211. Both particles were embedded in low-viscosity epoxy and thin sections (approximately 60-nm thick) were prepared using ultramicrotomy. High-resolution images, bright-field/dark-field images, and electron diffraction

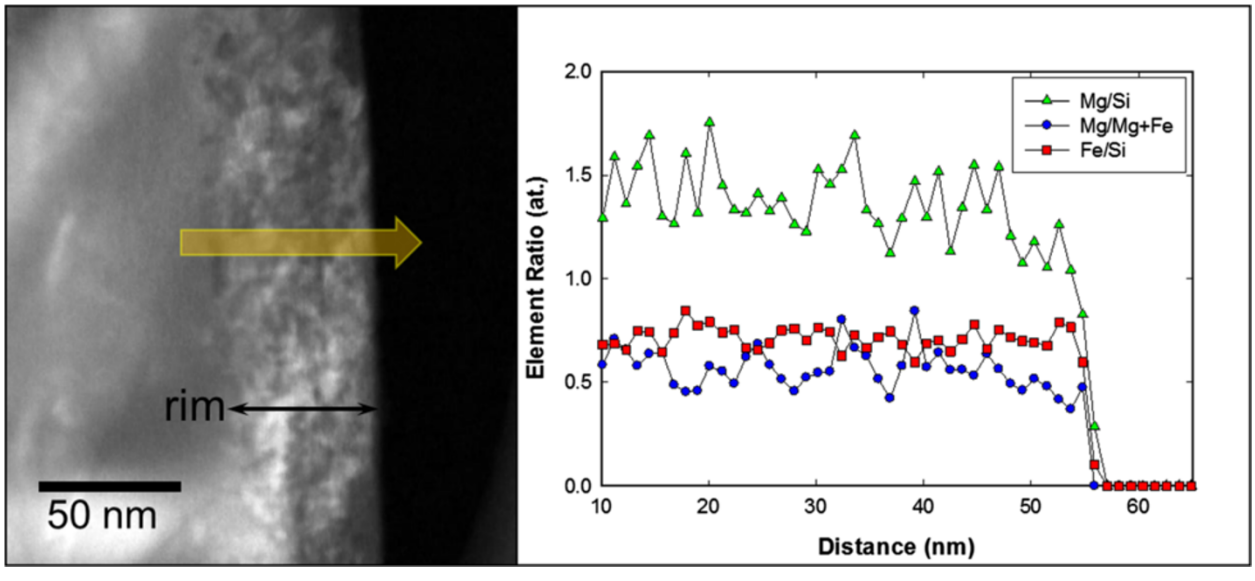

Figure 1 Dark-field STEM image of the disordered rim in particle RA-QD02-0125 and corresponding element ratio profiles. A dark-field STEM image of the disordered rim in particle RA-QD02-0125 (left) and corresponding element ratio profiles from the core through the rim of the grain, indicated by the yellow arrow in the STEM image (right).

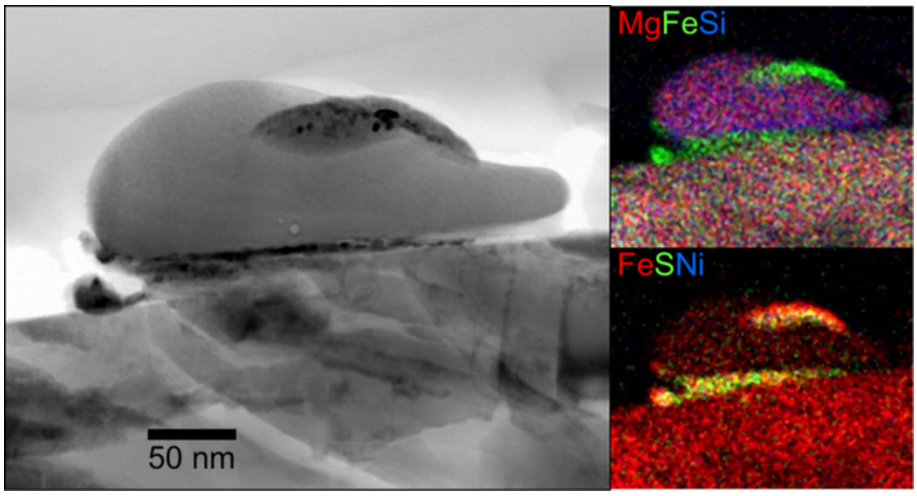

Figure 2 Bright-field STEM image of a melt droplet and RGB images showing the elemental distribution. A bright-field STEM image of a melt droplet on the surface of particle RA-QD02-0125 (left) and two composite RGB images showing the elemental distribution of the mixed silicate-sulfide melts (right).

data were obtained using a JEOL 2500SE 200-kV field-emission scanning transmission electron microscope (STEM; JEOL Ltd., Tokyo, Japan) equipped with a Thermo-Noran thin-window energy-dispersive x-ray (EDX) spectrometer (Thermo Fisher Scientific, Hudson, NH, USA). The JEOL 2500SE STEM was used to measure chemical compositions using EDX as well as to acquire quantitative elemental maps (spectrum images) of individual grains. Spectrum images contain a high-count EDX spectrum in each pixel, enabling the determination of quantitative element abundances in addition to displaying the spatial distribution of major and minor elements. For the spectrum imaging, we rastered a 4-nm-diameter incident probe (9 nA) with a dwell time of 50 μs/pixel to limit beam damage and element diffusion during the experiment. The size of the rastered area was typically 256 × 204 pixels at a magnification that was optimized to limit over- or under-sampling with the 4-nm probe. Successive image layers of each region were acquired and combined in order to achieve better than 10% counting statistics for major elements in each pixel. Element line profiles were extracted from the spectrum images.

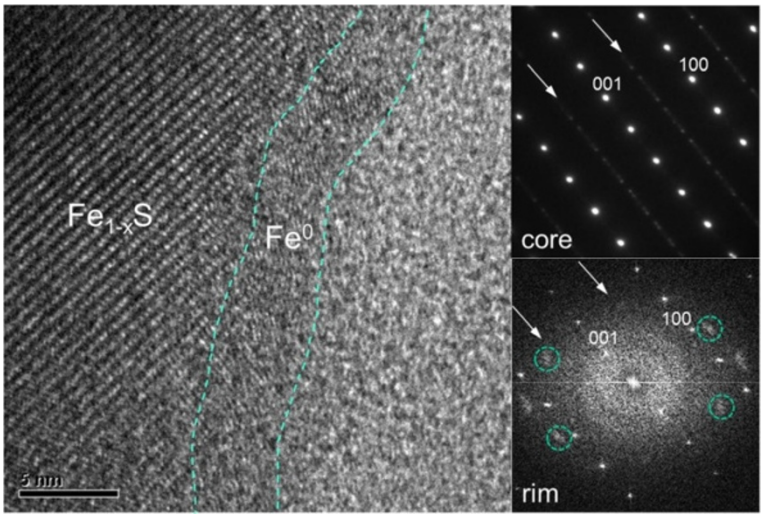

Figure 3 High-resolution TEM, selected-area electron diffraction, and FFT pattern of pyrrhotite grain in RA-QD02-0125. A high-resolution TEM of the space-weathered pyrrhotite grain in RA-QD02-0125 (left). The outermost surface of the grain is armored with a thin layer of nanophase Fe metal grains. The selected-area electron diffraction from the core of the grain (labeled 'core,' upper right) shows strong superstructure reflections (arrowed) that are absent in the fast-Fourier transform (FFT) pattern from the rim (labeled 'rim,' lower right). In addition, the FFT pattern from the rim shows reflections that are consistent with the (110) spacings of iron metal (small dashed circles).

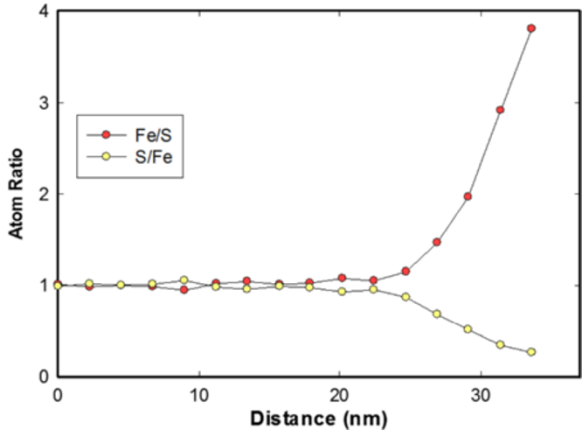

Figure 4 Quantitative element ratio plots across the space-weathered rim of a pyrrhotite grain. Quantitative element ratio plots across the space-weathered rim of a pyrrhotite grain exposed on the surface of particle RA-QD02-0125, which show a zone of sulfur depletion and iron enrichment in the outermost approximately 10 nm of the grain. Element ratio profiles were extracted from the spectrum images.

Results and discussion

Particle RA-QD02-0125 is an approximately 37-μm olivine single crystal that contains micrometer-sized inclusions of FeS and is surrounded by a microstructurally complex rim that shows a mottled contrast in TEM images. The particle is rounded in shape and has numerous submicrometer grains attached to its surface including pyrrhotite, albite, olivine, augite, orthopyroxene, and rare melt droplets. The composition of the olivine by TEM-EDX analyses is $Mg_{1.4}Fe_{0.6}SiO_4(Fo_{70})$ and is homogeneous. Solar flare tracks have not been observed within the olivine, and only an upper limit ($<10^9$ cm^{-2}) can be placed on the track density given the limitation imposed by the size of the fragments in the microtome thin sections. The particle is surrounded by a continuous approximately 50-nm thick, structurally disordered rim that is nanocrystalline with minor amorphous material between crystalline domains (Figure 1). We have not observed $npFe^0$ grains within the disordered rim. Compositional profiles obtained from the core of the grain through the rim show no major chemical differences except for the outermost 5 nm, which shows a slight Si enrichment (Figure 1). The adhering melt droplets are dominated by Fe sulfides, although a few melt droplets are immiscible mixtures of silicate glass (approximately chondritic) with Fe metal/Fe sulfide blebs (Figure 2).

One of the surface-adhering grains is a pyrrhotite grain that exhibits a strained rim on its exposed surface. Energy-dispersive x-ray mapping of the strained/disordered rim shows that the outer approximately 8- to 10-nm-wide zone is sulfur-depleted (Figure 3), with $npFe^0$ grains (<5 nm) decorating the outermost surface (Figure 4). The microstructure of the sulfur-depleted layer on the pyrrhotite grain in RA-QD02-0125 is similar to that observed in troilite irradiated with 4 kV He^+ ions to a fluence of approximately 10^{18} ions cm^{-2} (Loeffler et al. 2008; Keller et al. 2010). The pyrrhotite also displays a complex superstructure in its core that is absent in the sulfur-depleted rim (Figure 4). Prolonged ion irradiation has been shown to disorder pyrrhotite such that the superstructure reflections are lost (Christoffersen and Keller 2011).

Particle RA-QD02-0211 is an angular, approximately 41-μm olivine single crystal that contains micrometer-sized inclusions of FeS and solar flare particle tracks, and

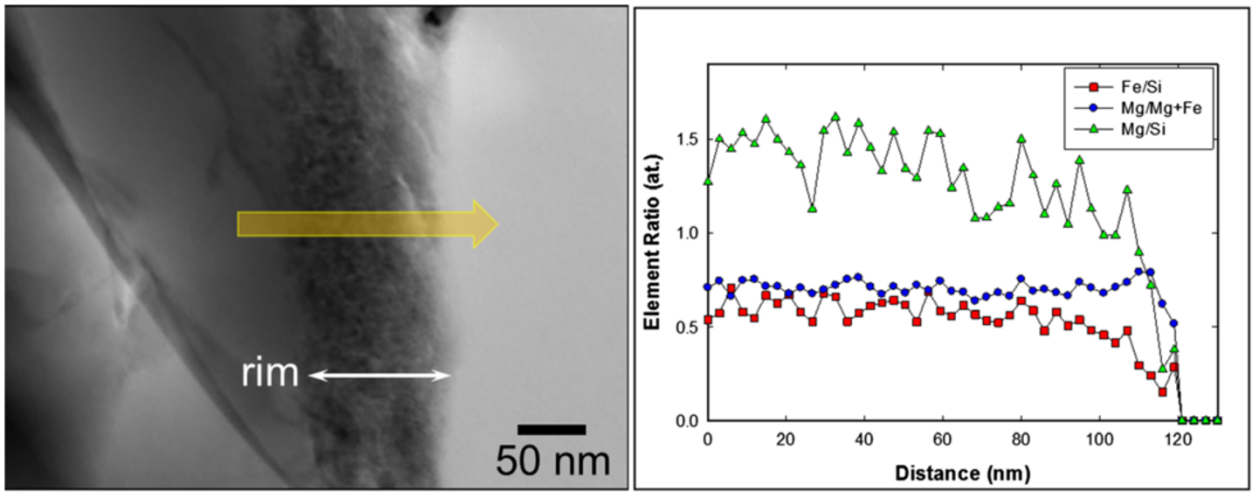

Figure 5 Bright-field STEM image of the rim in particle RA-QD02-0211 and corresponding element ratio profiles. A bright-field STEM image of the disordered rim in particle RA-QD02-0211 (left) and corresponding element ratio profiles from the core through the rim of the grain, indicated by the yellow arrow in the STEM image (right). The element profiles show a thin outermost later that is Si-enriched.

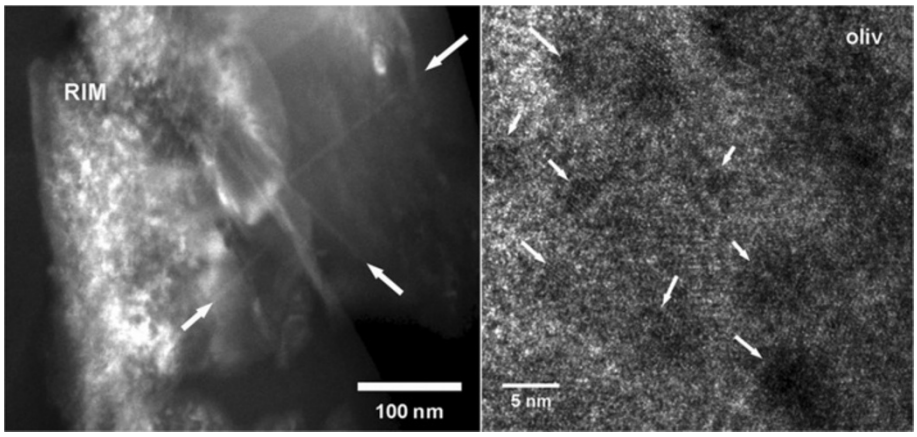

Figure 6 Dark-field STEM image of solar flare tracks in particle RA-QD02-0211 and high-resolution TEM image. A dark-field STEM image of the disordered rim in particle RA-QD02-0211 showing solar flare particle tracks (left, arrowed) and a high-resolution TEM image of the rim showing tiny (<5 nm diameter) nanophase Fe metal particles in the rim (right).

also shows a structurally disordered, approximately 100-nm-thick rim (Figure 5). The solar flare track density is approximately 2×10^{10} cm^{-2} (Figure 6). The disordered rim is nanocrystalline with minor amorphous material between crystalline domains. Quantitative element maps show that the outermost approximately 10 nm of the disordered rim is Si-rich with lower Mg/Si and Fe/Si than the core of the grain and likely represents vapor- or sputter-deposited material (Figure 5). We observed regions within the rim that contain npFe^0 particles (2 to 5 nm) in high-resolution TEM images, but they are not uniformly distributed throughout the rim (Figure 6).

Surface exposure

Solar flare energetic particles have a penetration depth of millimeter to centimeter and leave a trail of ionization damage in insulating materials. The solar flare track density correlates with exposure age as long as the grain was within a few centimeters of the parent body surface. From the analyses of lunar rock samples, the solar flare track production rate at 1 AU is approximately 6×10^5 year^{-1} for a 2π exposure (Blanford et al. 1975). Asteroid Itokawa has a semi-major axis of 1.324 AU and so we use the Blanford et al. rate for the Hayabusa samples. Based on this track production rate and assuming that the

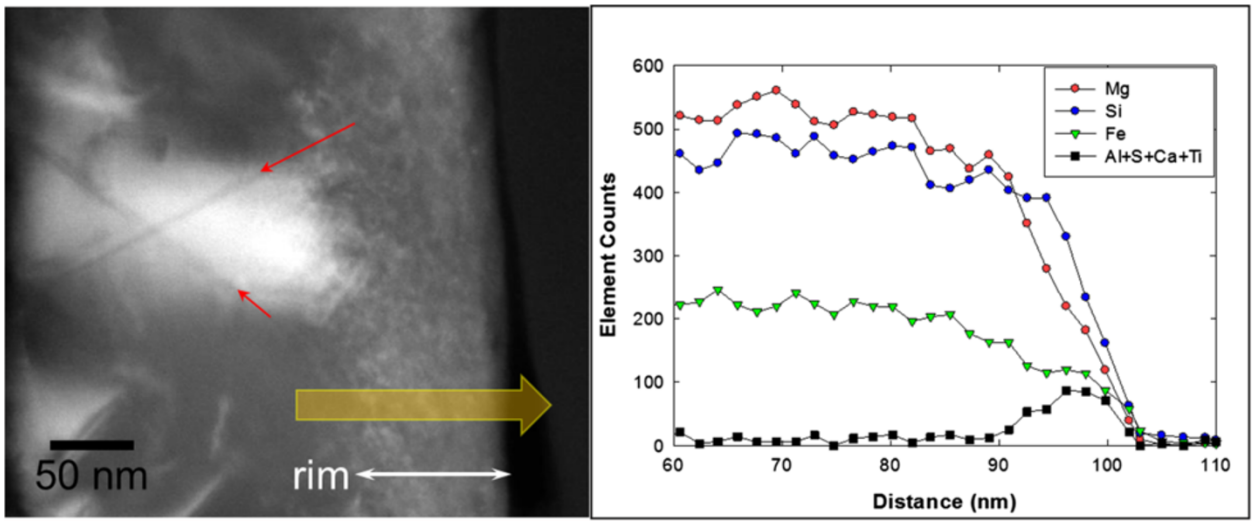

Figure 7 Dark-field STEM image of the disordered rim in a lunar olivine grain and element profiles. A dark-field STEM image of the disordered rim in an olivine grain from lunar soil 71501 (left). The olivine grain contains solar flare tracks (red arrows) with a density similar to that in RA-QD02-0211. The disordered rim shows a similar microstructure as the Hayabusa olivine grains, except that the outermost 10 to 15 nm of the rim is dominated by vapor-deposited material enriched in Ca, Al, Ti, and Si as shown in the element profiles through the rim (right), indicated by the yellow arrow in the STEM image.

particles had a single stage exposure in the Itokawa regolith, the track density in particle RA-QD02-0211 corresponds to a minimum surface exposure of approximately 3×10^4 years. We can only place an upper limit constraint on RA-QD02-0125 of $<10^3$ years, given its lack of observable tracks. Low track densities are difficult to measure in microtome thin sections owing to the chatter and disruption that results from the cutting process. We have developed a focused ion beam approach to preparing thin sections of Hayabusa particles that will enable more accurate measurement of track densities in the approximately 10^8 to 10^9 cm^{-2} range (Berger and Keller 2014).

The structurally disordered rims on the Hayabusa particles likely result from atomic displacement damage from solar wind ions given the similarity of the rim thickness compared to the implantation depth of solar wind ions. If the short surface exposure times we observe in these two particles are typical of Itokawa regolith grains in general, it implies that the optical effects of space weathering develop far more rapidly than previous estimates (Vernazza et al. 2009) by several orders of magnitude.

Comparison to olivine grains from lunar soils

We also analyzed microtome thin sections of olivine grains from a 20- to 45-μm-size fraction of Apollo 17 soil sample 71501 to compare the microstructures of these grains to those that we observed in the Hayabusa grains. The 71501 soil is classified as submature and we observed a range of solar flare densities (approximately 1 to 5×10^{10} cm^{-2}) in the grains. The 71501 olivines show disordered rims up to 100 nm wide that are highly strained, but only the outermost 10 to 15 nm is amorphous (Figure 7). We obtained compositional profiles across the rims of four olivines with similar track densities and all show an accumulation of elements that are not derived from the host olivine (e.g., Ca, Al, and Ti) in addition to a strong Si enrichment in the outer approximately 15 nm of the rims (Figure 7). The outmost layer likely represents a deposited layer from the condensation of impact-generated vapors similar to those observed on other lunar soil grains (Keller and McKay 1997). The underlying disordered material is compositionally similar to the core of the grain and is consistent with the solar-wind-damaged layers we observe on the Hayabusa olivine grains. Olivine grains from mature lunar soils show higher solar flare track densities (approximately 10^{11} cm^{-2}) and more extensive development of damaged rims, thicker rims of vapor-deposited material, and a higher density of $npFe^0$ particles.

Conclusions

Both Hayabusa particles described here record the effects of space weathering processes on Itokawa, which include the presence of microstructurally disordered rims that are still largely crystalline and thin (5 to 10 nm) outer layers of Si-rich vapor-deposited materials. Noguchi et al. (2011, 2013) proposed that the disordered rims observed on Itokawa particles largely result from solar wind radiation damage with a minor component of vapor-deposited elements. We arrive at a similar conclusion for the particles we analyzed. We observed solar flare tracks in only one of the particles and the track density is consistent with short surface exposures. The Hayabusa grains appear to lack the abundant melt spherules and vapor deposits that are common in lunar soil grains with a similar exposure history.

Abbreviations

EDX: energy-dispersive x-ray; FFT: fast-Fourier transform; $npFe^0$: nanophase Fe metal; STEM: scanning-transmission electron microscope; TEM: transmission electron microscope.

Competing interests

The authors have no competing financial interests or personal interests which may have impacted the interpretation of this data or the presentation of this information.

Authors' contributions

LPK and ELB contributed to data collection, interpretation, and manuscript preparation. Both authors read and approved the final manuscript.

Acknowledgements

This research was supported by a grant to LPK from the NASA Laboratory Analysis of Returned Samples (LARS) program. We gratefully acknowledge the samples allocated for this study from JAXA and the Hayabusa Curation Facility.

Author details

[1]Robert M Walker Laboratory for Space Science, Code KR, Astromaterials Research and Exploration Science, NASA Johnson Space Center, Houston, TX 77058, USA. [2]GeoControl Systems, Inc. - Jacobs JETS contract - NASA Johnson Space Center, Houston, TX 77058, USA.

Received: 27 February 2014 Accepted: 10 June 2014
Published: 15 July 2014

References

Abe M, Takagi Y, Kitazato K, Abe S, Hiroi T, Vilas F, Clark BE, Abell PA, Lederer SM, Jarvis KS, Nimura T, Ueda Y, Fujiwara A (2006) Near-infrared spectral results of asteroid Itokawa from the Hayabusa spacecraft. Science 312:1334–1338

Berger EL, Keller LP (2014) A novel hybrid ultramicrotomy/FIB-SEM technique: preparation of serial electron-transparent thin sections of a Hayabusa grain. Microsc Microanal, in press

Blanford GE, Fruland RM, Morrison DA (1975) Long-term differential energy spectrum for solar-flare iron-group particles. Proc Lunar Planet Sci 6:3557–3576

Chapman CR (2004) Space weathering of asteroid surfaces. Ann Rev Earth Planet Sci 32:539–567

Christoffersen R, Keller LP (2011) Space radiation processing of sulfides and silicates in primitive solar systems materials: insights from in-situ TEM ion irradiation experiments. Met Planet Sci 46:950–969

Gaffey MJ (2010) Space weathering and the interpretation of asteroid reflectance spectra. Icarus 209:564–574

Hiroi T, Abe M, Kitazato K, Abe S, Clark BE, Sasaki S, Ishiguro M, Barnouin-Jha OS (2006) Developing space weathering on the asteroid 25143 Itokawa. Nature 443:56–58

Keller LP, Clemett SJ (2001) Formation of nanophase iron in the lunar regolith. Lunar Planet Sci XXXII no:2097

Keller LP, McKay DS (1997) The nature and origin of rims on lunar soil grains. Geochim Cosmochim Acta 61:2331–2340

Keller LP, Loeffler MJ, Christoffersen R, Dukes CA, Rahman Z, Baragiola RA (2010) Irradiation of FeS: implications for the lifecycle of sulfur in the interstellar medium and presolar FeS grains. Lunar Planet Sci XLI no:1172

Loeffler MJ, Dukes CA, Chang WY, McFadden LA, Baragiola RA (2008) Laboratory simulations of sulfur depletion at Eros. Icarus 195:622–629

Miyamoto H, Yano H, Scheeres DJ, Abe S, Barnouin-Jha O, Cheng AF, Demura H, Gaskell RW, Hirata N, Ishiguro M, Michikami T, Nakamura AM, Nakamura R, Saito J, Sasaki S (2007) regolith migration and sorting on asteroid Itokawa. Science 316:1011–1014

Nakamura T, Noguchi T, Tanaka M, Zolensky ME, Kimura M, Nakato A, Ogami T, Ishida H, Tsuchiyama A, Yada T, Shirai K, Okazaki R, Fujimura A, Ishibashi Y, Abe M, Okada T, Ueno M, Mukai T (2011) Mineralogy and major element abundance of the dust particles recovered from Muses-C Regio on the asteroid Itokawa. Lunar Planet Sci XXXXII no:1766

Noguchi T, Tsuchiyama A, Hirata N, Demura H, Nakamura R, Miyamoto H, Yano H, Nakamura T, Saito J, Sasaki S, Hashimoto T, Kubota T, Ishiguro M, Zolensky ME (2010) Surface morphological features of boulders on Asteroid 25143 Itokawa. Icarus 206:319–326

Noguchi T, Kimura M, Hashimoto T, Konno M, Nakamura T, Zolensky ME, Okazaki R, Tanaka M, Tsuchiyama AN, Aiko OT, Ishida H, Sagae R, Tsujimoto S, Matsumoto T, Matsuno J, Fujimura A, Abe M, Yada T, Mukai T, Ueno M, Okada T, Shirai K, Ishibashi Y (2013) Space weathered rims found on the surfaces of the Itokawa dust particles. Met Planet Sci 46:950–969

Noguchi T, Nakamura T, Kimura M, Zolensky ME, Tanaka M, Hashimoto T, Konno M, Nakato A, Ogami T, Fujimura A, Abe M, Yada T, Mukai T, Ueno M, Okada T, Shirai K, Ishibashi Y, Okazaki R (2011) SEM and TEM observation of the surfaces of the fine-grained particles retrieved from the MUSES-C region on the asteroid 25143 Itokawa. Lunar Planet Sci XXXXII no:1596

Takeuchi H, Miyamoto H, Oku M (2009) Distributions and morphological characteristics of bright spots on boulders covering the surface of asteroid Itokawa. Lunar Planet Sci XV no:1566

Tsuchiyama A, Ebihara M, Kimura M, Kitajima F, Kotsugi M, Ito S, Nagao K, Nakamura T, Naraoka H, Noguchi T, Okazaki R, Uesugi K, Uesugi M, Yurimoto H, Ireland TR, Sandford SA, Zolensky ME, Fujimura A, Abe M, Yada T, Mukai T, Okada T, Ishibashi Y, Shirai K, Ueno M, Kawaguchi J, Yoshikawa M (2011) Preliminary examination of particles recovered from the surface of the asteroid 25143 Itokawa by the Hayabusa Mission. Lunar Planet Sci XXXXII no:1788

Vernazza P, Binzel RP, Rossi A, Fulchignoni M, Birlan M (2009) Solar wind as the origin of rapid reddening of asteroid surfaces. Nature 458:993–995

Zhang S, Keller LP (2011) Space weathering effects in lunar soils: the roles of surface exposure time and bulk chemical composition. Lunar Planet Sci XLII no:1947

doi:10.1186/1880-5981-66-71
Cite this article as: Keller and Berger: **A transmission electron microscope study of Itokawa regolith grains.** *Earth, Planets and Space* 2014 **66**:71.